Supporting Material

An integrated photo-rechargeable $ZnMoO_4$//reduced graphene oxide hydrogel supercapacitor

Yu Wang[a], Rong Zhong[a], Chirstopher Bassanyin[a], Jiake Li[a,b,*], Hedong Jiang[a], Xin Liu[a], Ziyi Chen[a], Pingchun Guo[a], Hua Zhu[c], Yanxiang Wang[a]

Corresponding Author: Jiake Li, E-mail: jiakeli.jci@163.com

a School of Materials Science and Engineering, Jingdezhen Ceramic University, Jiangxi, 333403, China

b Jiangxi Key Laboratory of Advanced Ceramic Materials, Jiangxi, 333403, China

c School of Mechanical and Electrical Engineering, Jingdezhen Ceramic University, Jiangxi, 333403, China

2 Experimental

2.4 Characterization

(1) XRD test characteristic data:

The voltage is 40 kV, the current is 40 mA, the step scan size is 0.02° , and the counting time is 0. 2 second/step.

(2) The sample preparation process for electronic microscopy

Take a small amount of $ZnMoO_4$ powder (about 1-2 mg) and place it in a centrifuge tube. Add 1 - 2 mL of anhydrous ethanol and sonicate for 15 minutes, and then use a micropipette to extract the upper uniform suspension and dry it under an infrared lamp.The GO film sample was obtained by freeze - drying the GO suspension, and the rGH dry gel sample was obtained by freeze - drying the aqueous rGH gel.A mild gold - spraying treatment was performed for all samples before observation.

(3) XPS test characteristic data:

Using a monochromatic Al Kα X-ray source (hv=1486.6 eV), the material used for calibration is high-purity Au (Au $4f_{7/2}$ = 84.0 eV).

In Avantage software, after importing the data and subtracting the background (usually Shirley background), Gaussian - Lorentz mixed peaks are added according to the possible chemical states of the elements. Physical constraints are then applied to the spacing and area ratio of their spin - orbit doublets. Finally, iterative fitting is employed to achieve the best match between the synthesized spectrum and the experimental data.

(4) FTIR and Raman test characteristic data:

The FTIR test was carried out using a Nicolet 5700 spectrometer. A total of 32 scans were performed in transmission/attenuated total reflection mode with a resolution of 4 cm^{-1}. The resolution of the Raman spectroscopy was 1 cm^{-1}, and three scans were conducted.

(5) Nitrogen adsorption-desorption isotherm(BET) test characteristic data:

The specific surface area test was carried out using a Micromeritics ASAP 2460 physical adsorption instrument, with high - purity nitrogen gas serving as the adsorbate. Before testing, approximately 100 mg of the rGH sample should be placed in a sample tube, and then a high - vacuum (vacuum degree < 10 μmHg) degassing treatment should be performed at 120 °C for 7 hours to thoroughly clean the sample's surface.

3 Results and discussion

3.1 Phase compositional and structural analyses of as-synthesized $ZnMoO_4$

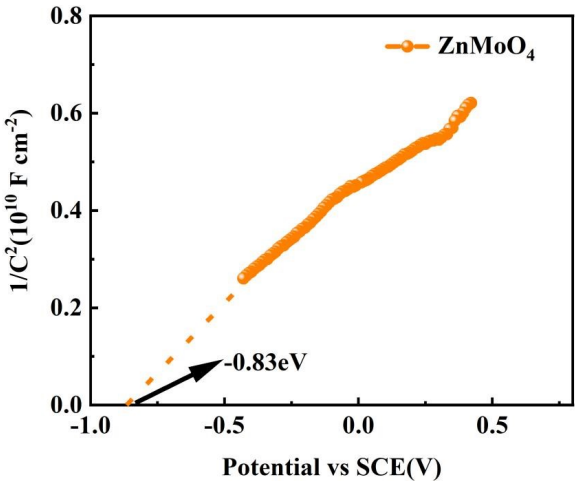

Fig. S1 Mott-Schottky plots for $ZnMoO_4$ (testing frequency:1000 Hz)[1]

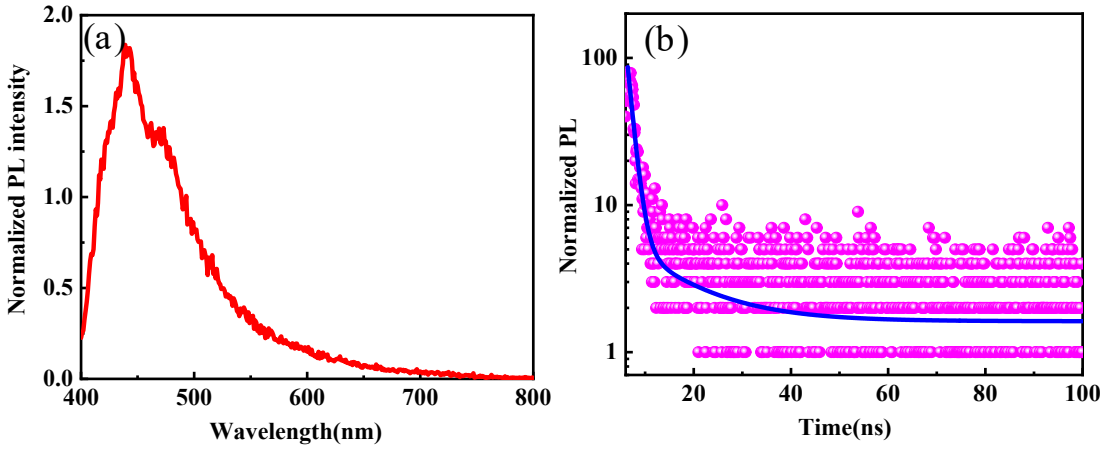

Fig. S2 (a) PL spectrum and (b) TRPL spectrum of $ZnMoO_4$

3.4 Photoelectric properties of $ZnMoO_4$//rGH photorechargeable supercapacitor

The specific capacities of the supercapacitors with different mass ratios of $ZnMoO_4$ to rGH are shown in Table S1. With mass ratios ranging from 1.5:1 to 4:1, the specific capacities first increase and then decrease. When the mass ratio of $ZnMoO_4$ to rGH is 2.5:1, the supercapacitor has the highest specific capacity, and the values are 115.06 F g^{-1} and 156.09 F g^{-1} without and with illumination, respectively.

The mass ratios of $ZnMoO_4$ to rGH are too small, the photoanode films are relatively thinner. For example, the mass ratio of $ZnMoO_4$ to rGH is 1.5:1, the thickness of the photoanode film is approximately 10 μm, which leads to lower light absorption and photoelectric performance.[2] When the mass ratios are too large, the photoanode films are relatively thicker. For example, the mass ratio of $ZnMoO_4$ to rGH is 4:1, the thickness of the photoanode film is approximately 35 μm, which results in carrier recombination, thereby reducing the specific capacity.[3] When the mass ratio of $ZnMoO_4$ to rGH is 2.5:1, the photoanode film has an appropriate thickness of approximately 20 μm. It can sufficiently harvest light energy, convert it into electric energy, thereby minimize carrier recombination, and resultantly enhance the specific capacity.[4]

Table S1 Effect of mass ratios of $ZnMoO_4$ to rGH in the electrodes on the specific capacities of the supercapacitors (with a current density of 0.5 A. g^{-1})

$ZnMoO_4$:rGH	1.5:1	2:1	2.5:1	3:1	4:1
Without illumination(F g^{-1})	60.3	93	115.06	106	80
With illumination(F g^{-1})	83.5	100	156.09	138	98.5

Notes: The area density of $ZnMoO_4$ photoanode and rGH cathode are 8.25 mg cm^{-2} and 3.30 mg cm^{-2}, respectively.

In order to estimate the contribution of diffusion and capacitive processes to the specific capacity, it is obtained from the equation $i = k_1v + k_2v^{1/2}$, where i is the current value (A g^{-1}), v is the scanning rate (V s^{-1}), k_1v is the capacitance-controlled process and k_2v is the diffusion-controlled process. Fig. S3 shows the capacitance contribution of the supercapacitor with electric charging and photoelectric synergistic charging at different scanning rates. When the scanning rates are 10 mV s^{-1}, 20 mV s^{-1}, 50 mV s^{-1} , and 100 mV s^{-1}, the capacitive contribution is 22%, 24%, 40% and 63% without illumination, and is 23%, 26%, 41% and 64% with illumination, respectively. The capacitive contribution increases with the increase of the scanning rates due to the increase of the charge transfer. In addition, at the same scanning rate, under the conditions of electric charging and photoelectric synergistic charging, the contribution rates of capacitance are approximately equal.

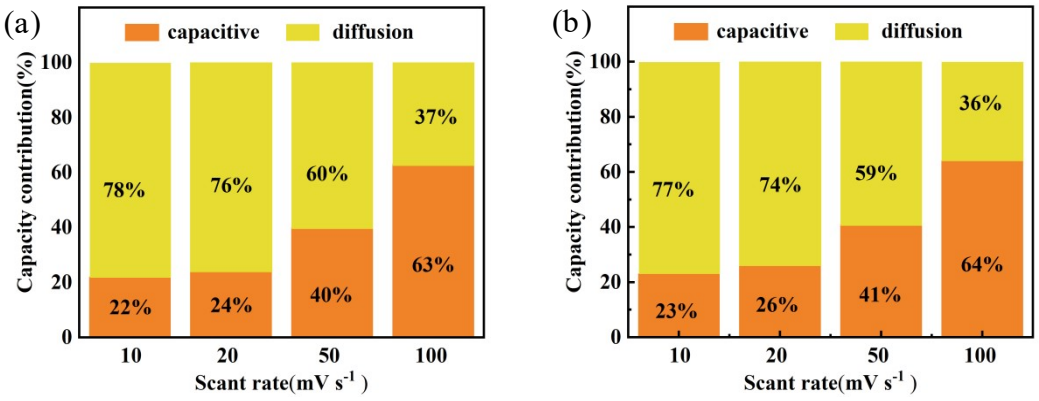

Fig. S3 Capacitance contribution of the supercapacitor at different scanning rates (a) electric charging, (b) photoelectric synergistic charging

Fig. S4 shows the photocurrent test of $ZnMoO_4$ electrode under different bias

voltages (including no bias). It can be seen from the figure that a clear net photocurrent signal can be observed under illumination, confirming the effective charge generation and separation phenomenon. As the positive bias increases, the photocurrent significantly increases, indicating that the external electric field further promotes the separation and transport of electron hole pairs. In addition, the current under illumination is significantly higher than that under dark current, the Faraday reaction under illuminated conditions is stronger than that in the dark conditions.

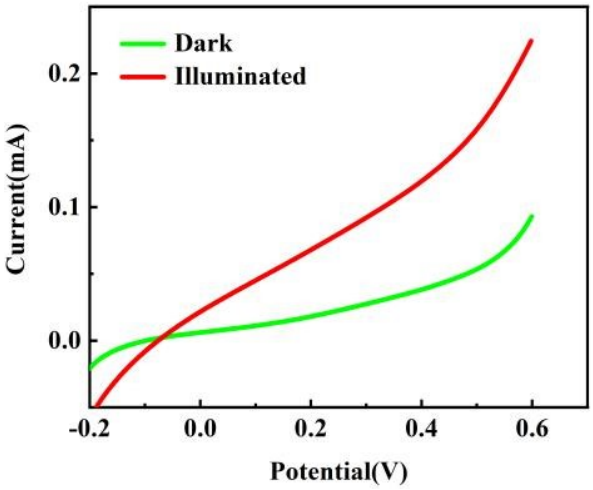

Fig. S4 Photocurrent testing of $ZnMoO_4$ electrode

Table S2 shows photoelectrochemical performance of the supercapacitors about similar literature and this work. It can be seen from Table S2 that the as-synthesized device has a higher photocharging voltage (0.8 V), the specific capacity (46.8 F g^{-1}) , the energy density (4.2 Wh kg^{-1}), and PCE (0.02%) only photocharging 17 min compared with similar literature, indicating that the as-synthesized device has better comprehension performance.

Table S2 Comparison of photoelectrochemical performance between similar literature and this work

Photorechargeable energy storage devices	PCE	The specific capacity	Photo-votage	Energy density	Ref.
Photorechargeable hybrid halide perovskite supercapacitors	0.02%@ 20 mW cm^{-2}		0.3 V	0.16 Wh kg^{-1}	5
Photo-rechargeable asymmetric supercapacitors based on nickel–cobalt sulfide on titania as novel photo-active electrodes	100 mW cm^{-2}	0.9 F cm^{-2}	0.6 V	/	6
Vanadium dioxide–zinc oxide stacked photocathodes for photo-rechargeable zinc-ion batteries	12 mW cm^{-2}	367mAh g^{-1}	0.9 V	/	7
Preparation of photorechargeable asymmetric supercapacitors using S,W-codoped titania: experimental and theoretical insights	100 mW cm^{-2}	179 mF cm^{-2}	0.4 V	6.21 Wh cm^{-2}	8
Photorechargeable zinc-ion capacitor using 2D graphitic carbon nitride	0.01%@ 50 mW cm^{-2}	11.3 F g^{-1}	0.8 V	0.7 Wh kg^{-1}	9
An integrated photo-rechargeable $ZnMoO_4$//reduced graphene oxide hydrogel supercapacitor	0.02%@ 95 mW cm^{-2}	46.8 F g^{-1}	0.8 V	4.2 Wh kg^{-1}	This work

Fig. S5 shows XRD patterns of the $ZnMoO_4$ photoanode before and after 10000 cycles. It can be seen that the diffraction peaks did not change before and after cycling, indicating that the constructed device has good photoelectrochemical stability.

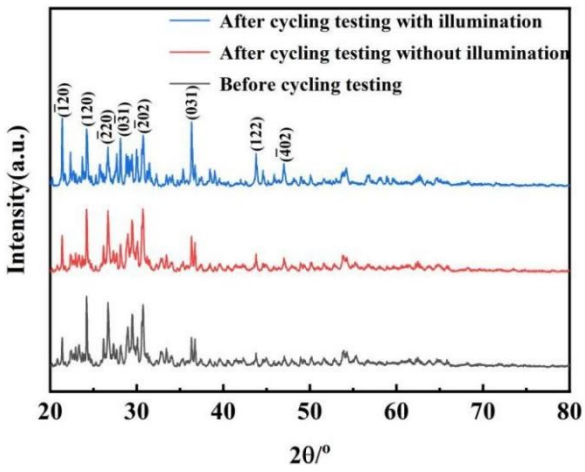

Fig. S5 XRD patterns of the $ZnMoO_4$ photoanode before and after 10000 cycles

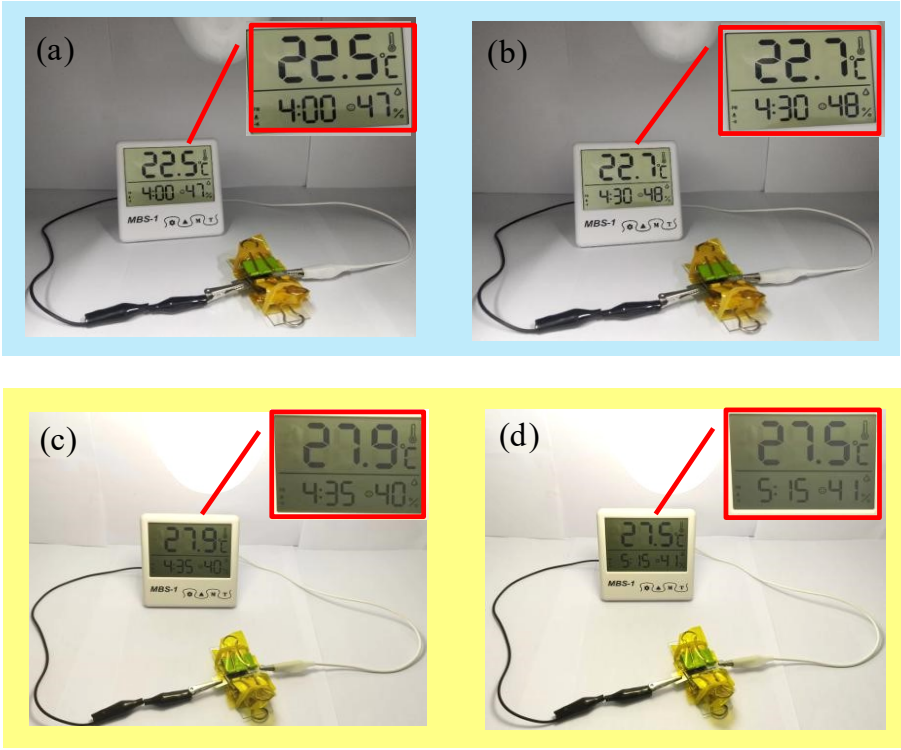

Fig. S6 Photographs representing an electronic device driven by the as-constructed supercapacitor through the whole process from (a) start to (b) end without illumination, as well as (c) and (d) with illumination, respectively.

References

1 X. Guo, L. Fan, Y. Liu and Z. Jin, *Renewable Energy*, 2024, **222**, 119877.

2 N. Murakami and R. Watanabe, *ACS Comb. Sci.*, 2020, **22**, 791–795.

3 A. Ansón-Casaos, J. C. Ciria, C. Martínez-Barón, B. Villacampa, A. M. Benito and W. K. Maser, *Int. J. Hydrogen Energy*, 2024, **52**, 1146–1158.

4 S. Hernández, G. Saracco, G. Barbero and A. L. Alexe-Ionescu, *J. Electroanal. Chem.*, 2017, **799**, 481–486.

5 R. Kumar, A. Kumar, P. S. Shukla, G. D. Varma, D. Venkataraman and M. Bag, *ACS Appl. Mater. Interfaces*, 2022, **14**, 35592–35599.

6 M. Najafi, M. Mohsen Momeni and B.-K. Lee, *Chem. Eng. J.*, 2024, **493**, 152423.

7 B. Deka Boruah and M. De Volder, *J. Mater. Chem. A*, 2021, **9**, 23199–23205.

8 M. M. Momeni, H. M. Aydisheh, B.-K. Lee, H. Farrokhpour and M. Najafi, *J. Alloys Compd.*, 2023, **960**, 170722.

9 B. D. Boruah, A. Mathieson, B. Wen, C. Jo, F. Deschler and M. De Volder, *Nano Lett.*, 2020, **20**, 5967–5974.